Angular momentum population in the fragmentation of ^{208}Pb at 1 GeV/nucleon

M. Pfützner,[1,*] P. H. Regan,[2] P. M. Walker,[2] M. Caamaño,[2] J. Gerl,[3] M. Hellström,[3,4] P. Mayet,[3] K. -H. Schmidt,[3] Zs. Podolyák,[2] M. N. Mineva,[4] A. Aprahamian,[2,†] J. Benlliure,[5] A. M. Bruce,[6] P. A. Butler,[7] D. Cortina Gil,[3] D. M. Cullen,[7,‡] J. Döring,[3] T. Enquist,[3] C. Fox,[7] J. Garcés Narro,[2] H. Geissel,[3] W. Gelletly,[2] J. Giovinazzo,[9] M. Górska,[3] H. Grawe,[3] R. Grzywacz,[10] A. Kleinböhl,[3] W. Korten,[11] M. Lewitowicz,[12] R. Lucas,[11] H. Mach,[13] C. D. O'Leary,[7] F. De Oliveira,[12] C. J. Pearson,[2] F. Rejmund,[8] M. Rejmund,[8] M. Sawicka,[1] H. Schaffner,[3] Ch. Schlegel,[3] K. Schmidt,[3] Ch. Theisen,[11] F. Vivès,[3] D. D. Warner,[14] C. Wheldon,[2,7] H. J. Wollersheim,[3] and S. Wooding[2,3]

[1]*Institute of Experimental Physics, Warsaw University, PL-00681 Warsaw, Poland*
[2]*Department of Physics, University of Surrey, Guildford GU2 7XH, United Kingdom*
[3]*GSI, Planckstrasse 1, D-64291 Darmstadt, Germany*
[4]*Division of Cosmic and Subatomic Physics, Lund University, SE-22100, Sweden*
[5]*Departamento Física de Partículas, University of Santiago de Compostela, Spain*
[6]*School of Engineering, University of Brighton, Brighton BN2 4GJ, United Kingdom*
[7]*Oliver Lodge Laboratory, Department of Physics, University of Liverpool, Liverpool L69 3BX, United Kingdom*
[8]*IPN, F-91406 Orsay Cedex, France*
[9]*CEN Bordeaux-Gradignan/CNRS, F-33175 Gradignan Cedex, France*
[10]*Department of Physics and Astronomy, University of Tennessee, Knoxville, Tennessee 37996*
[11]*CEA Saclay, DSM/DAPNIA/SPhN, F-91191 Gif-sur-Yvette Cedex, France*
[12]*GANIL, BP 5027, F-14021 Caen Cedex, France*
[13]*Department of Radiation Sciences, Uppsala University, S-61182 Nyköping, Sweden*
[14]*CLRC Daresbury Laboratory, Warrington WA4 4AD, United Kingdom*

(Received 29 May 2001; revised manuscript received 15 February 2002; published 23 May 2002)

A systematic study of the population probabilities of microsecond isomers produced following the fragmentation of ^{208}Pb projectiles at 1 GeV/nucleon has been undertaken at the SIS/FRS facility at GSI Darmstadt. Gamma decays from approximately 20 isomeric states, mainly in the rare-earth and transitional nuclei with $A \sim 180$, were identified and the corresponding isomeric ratios deduced. The results are compared with a model based on the statistical abrasion-ablation description of relativistic fragmentation and simple assumptions concerning gamma cascades in the final nucleus (sharp cutoff). The model is found to represent an upper limit for the population of isomeric states in relativistic projectile fragmentation.

DOI: 10.1103/PhysRevC.65.064604 PACS number(s): 25.70.Mn, 23.20.−g

I. INTRODUCTION

The application of projectile fragmentation reactions at intermediate and relativistic energies to studies of nuclei far from stability has made substantial progress over the last few years. The main feature of this technique—namely, kinematical focusing allowing the fast and chemically insensitive separation of products in a magnetic spectrometer, coupled together with complete and unambiguous identification in-flight of each individual ion—results in an extremely sensitive selection of rare residual channels, as demonstrated by the recent identification of the long sought after doubly magic nuclei $^{100}_{50}$Sn$_{50}$ [1], $^{78}_{28}$Ni$_{50}$ [2], and $^{48}_{28}$Ni$_{20}$ [3]. As a consequence, this technique has been chosen as the basis of one of the two complementary types of second-generation radioactive beam facilities which are currently being planned.

Another advantageous feature of fragmentation reactions is the relatively high probability of populating isomeric states [4–11]. The combination of sensitivity and universality offered by projectile fragment separators, together with efficient, delayed gamma-ray spectroscopy of the selected and identified ions in metastable states, opens attractive possibilities for obtaining nuclear structure information on nuclei far from the stability line which are presently inaccessible with other experimental techniques. Although this method is limited to decays of isomeric states with half-lives between approximately 10 ns and 1 ms, its application has already provided interesting results. For example, the identification of the 8^+ isomer in ^{78}Zn [12] establishes this as the closest nucleus to the doubly magic ^{78}Ni with known excited states. The results from that experiment support the idea that $N=50$ is a closed shell for nickel isotopes. Another example is the observed decay of a $K^\pi=(10^-)$ isomer in ^{190}W, which represents the most neutron-rich tungsten isotope with identified excited states [13] and puts new limits on the region of K isomers for heavy transitional isotopes.

The basic properties of fragmentation reactions, such as the production cross sections and/or momentum distributions of the reaction products, knowledge of which is crucial for the design and optimal operation of a fragment separator, are rather well known [14–16]. In contrast, experimental infor-

*Corresponding author. Electronic address: pfutzner@mimuw.edu.pl
†Permanent address: Department of Physics, University of Notre Dame, South Bend, Indiana, 46556.
‡Present address: Schuster Laboratory, University of Manchester, Manchester M13 9PL, UK.

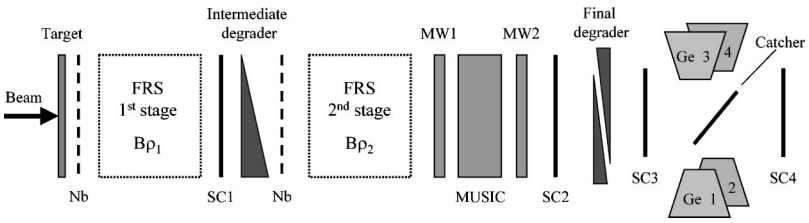

FIG. 1. Schematic drawing of all the materials and detectors placed in the FRS beamline during the experiment. Details are given in the text.

mation on the population of states as a function of angular momentum in fragmentation reactions is far from complete. Recently, probabilities for the production of a number of microsecond isomers produced in the quasifragmentation reactions of ^{112}Sn, ^{92}Mo, and ^{86}Kr beams at energy of about 60 MeV/nucleon have been published [5,8,17,18]. However, for projectile energies above 100 MeV/nucleon, much less information is known. For this ''relativistic'' energy domain, prior to the current work, the only reported results to our knowledge are the population probabilities for the ^{43}Sc isomer produced by the fragmentation of a ^{46}Ti beam [10] and for a few microsecond isomers identified among the fragmentation products of a ^{238}U beam at 1 GeV/nucleon [11].

Motivated by the lack of data on the one hand and by the prospects of forming and utilizing beams of exotic nuclei in metastable states [19] on the other, we have performed a study of the population of microsecond isomers following the projectile fragmentation of a ^{208}Pb beam at 1 GeV/nucleon at the SIS/FRS facility at GSI Darmstadt. A number of new isomers have been identified in this experiment and some interesting cases have already been published elsewhere [13,20–27]. In the present paper we report on results obtained for approximately 20 previously reported isomers which cover a broad range in atomic mass, excitation energy, and angular momentum. In the next section a detailed description of the experimental method and identification procedure is given. The following section deals with the analysis of the data and presents the results. In Sec. IV a simple model of isomeric population, based on the abrasion-ablation theory of the fragmentation process, is introduced. A comparison of the measured values with model predictions is discussed in Sec. V.

II. EXPERIMENTAL TECHNIQUE

A. Setup

The nuclei of interest were produced following the fragmentation of a 1 GeV/nucleon ^{208}Pb primary beam, delivered by the SIS synchrotron, onto a 1.6 g/cm^2 beryllium production target, which was located at the entrance of the GSI projectile fragment separator FRS [28]. The average primary beam intensity, as measured by a secondary electron monitor, varied between 1×10^6 ions per spill when fragments close to stability were selected and 2×10^8 ions per spill at settings on nuclei very far from the line of stability. The typical length and repetition period of a spill were 4 and 10 s, respectively.

The FRS was operated in the standard achromatic mode with an aluminum wedge-shaped degrader at the intermediate focal plane (see Fig. 1). The thickness of the degrader at the optical axis was set to 4.4 g/cm^2 and was kept constant throughout the experiment.

In order to maximize the electron stripping, niobium foils of thickness 221 mg/cm^2 and 108 mg/cm^2 were mounted downstream from the target and the degrader, respectively. The probability of an ion being fully stripped of electrons in both sections of the FRS was calculated with the code GLOBAL [29]. It was found that the corresponding values were typically about 96% and 88%. Predictions of the GLOBAL code were tested by measuring the intensities of the fully stripped, H-like and He-like charge states of the primary beam, and an excellent agreement between calculated and measured values was found.

In-flight identification of ions in the second stage of the FRS was achieved by a standard detector setup, as shown schematically in Fig. 1. At the intermediate focal plane, upstream from the degrader, a 5-mm-thick plastic scintillator (SC1) was mounted. This served for both time-of-flight (TOF) and position measurements. The latter, measured in the horizontal (dispersive) direction, was determined from the time difference between signals read from the left and right ends of the SC1 scintillator. The particle identification detectors at the final focus consisted of (i) two multiwire proportional chambers (MW1, MW2), yielding horizontal and vertical positions, (ii) a fourfold ionization chamber (MUSIC) providing energy-loss information ΔE, and (iii) a plastic scintillator (SC2) of 5 mm thickness which delivered the second TOF signal and the trigger for the acquisition system.

After passing the identification setup, the ions were slowed down in an aluminum degrader of thickness between 4.4 g/cm^2 and 5 g/cm^2 (depending on the FRS setting), and were finally implanted into a 4-mm-thick aluminum catcher. Two additional plastic scintillators (SC3, SC4) were mounted on either side of the catcher and used to verify that all selected ions were stopped in the catcher. The energy-loss signal from the SC3 detector was also used for off-line suppression of events resulting from charge-changing nuclear interactions of ions during the slowing down process. The catcher plate was of dimensions 20 cm wide and 10 cm high and was thus large enough to stop all the heavy fragments transmitted simultaneously at any one FRS setting. The catcher was surrounded by three segmented clover germanium detectors from the EXOGAM Collaboration [30] and a large-volume GSI ''Super Clover,'' mounted as close as possible to the catcher, but without blocking the heavy-ion trajectories. Each detector consisted of four separate germanium crystals. Out of these 16 available individual gamma channels, only 14 were included in the off-line analysis presented in the current study (two channels were rejected be-

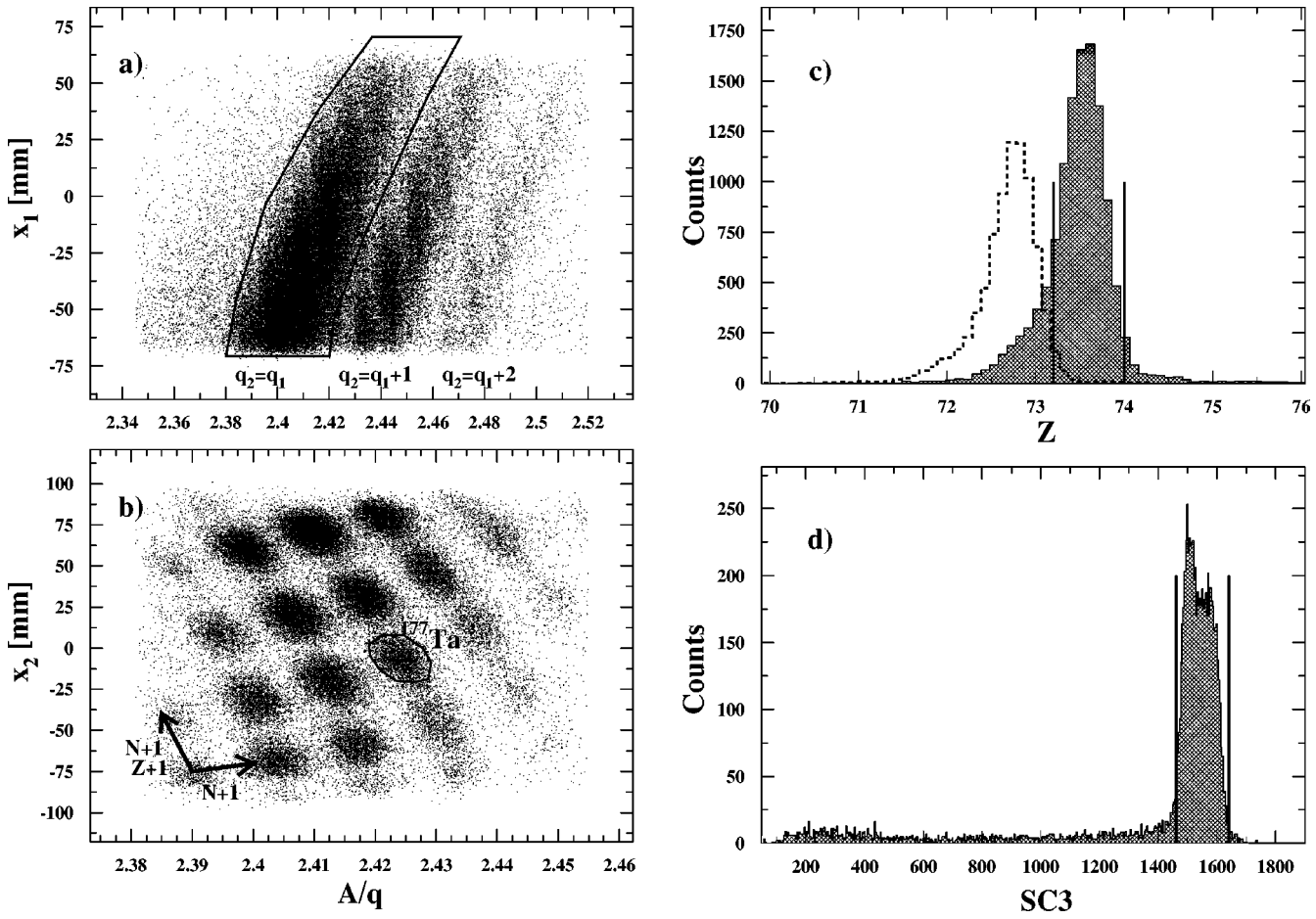

FIG. 2. Steps in the heavy-ion identification procedure. Only a sample of the full statistics is shown. (a) Position at the intermediate focus vs A/q ratio measured in the second stage of the FRS. A contour line shows the selection of events with the same ionic charge in both FRS stages. (b) Position at the final focus vs A/q for ions selected in step (a). Events for ^{177}Ta ions are shown by the contour line. (c) Spectrum of Z values, given by the ionization chamber, for events selected in steps (a) and (b). For comparison, the corresponding spectrum for ^{174}Hf is shown by the dashed line. A selection gate for tantalum ions is indicated. (d) A raw energy-loss spectrum from the SC3 scintillator for events selected in steps (a), (b), and (c). The final gate, which chooses those fully stripped ^{177}Ta ions which were *not* destroyed, is shown.

cause of timing or gain instability problems).

For the setting-up and tuning of all the identification detectors and the spectrometer itself, a set of measurements with low intensity primary beam (^{208}Pb) of different energies was performed prior to the isomer production runs. This allowed an absolute calibration of the TOF and energy loss (ΔE), as well as the horizontal positions at the intermediate and final focuses (x_1 and x_2, respectively).

B. Identification of heavy ions

From the ion-optical properties of the achromatic mode of the FRS, it follows that the magnetic rigidity $B\rho_2$ of each particle in the second stage of the FRS can be calculated from the expression

$$B\rho_2 = B\rho_0\left(1 - \frac{x_2 - V_2 x_1}{D_2}\right), \tag{1}$$

where $B\rho_0$ is the magnetic rigidity of particles at the optical axis, given by the magnetic fields of the dipole magnets and their radii. The magnification V_2 and dispersion D_2 of the second stage were 1.094 and 6969 mm, respectively.

The mass-to-charge ratio A/q is then given by

$$A/q = \frac{e}{u\,c}\,\frac{B\rho_2}{\beta\,\gamma}, \tag{2}$$

where e is the elementary charge, u is the atomic mass unit, β is the ratio of the velocity of an ion, determined from the TOF, to the speed of light c, and γ is the Lorentz factor ($\gamma = 1/\sqrt{1-\beta^2}$).

The steps in the heavy-ion identification procedure are illustrated in the four parts of Fig. 2, which show data collected while the FRS was tuned for the optimal transmission of ^{177}Ta.

Initially, the position x_1 is plotted against A/q [Fig. 2(a)] allowing a selection in terms of the charge-state difference between the first and second FRS sections. The group of events marked by a polygon represents ions whose charge state remained unchanged while passing through the degrader and detector materials at the intermediate focus.

These events predominantly correspond to fully stripped ions contaminated by some H-like ions. The contribution from He-like ions is negligible. The neighboring group of events represents ions which picked up an electron at the intermediate focus. Here, the main contribution comes from fully stripped ions emerging from the target stripper which change to the H-like state in the second stage.

For events selected by the condition in Fig. 2(a), the position x_2 versus A/q is plotted [see Fig. 2(b)], which highlights the good separation by both element and isotope. A comparison with the ion-optical Monte Carlo simulation MOCADI [31] can be used to determine the identity of the selected nuclides. (As will be discussed later in more detail, this identification is fully confirmed by the observation of the gamma rays depopulating known isomers present in the selection.) From the MOCADI simulation it follows that for each ion with mass A and atomic number Z, identified in Fig. 2(b), there is a small contamination from a nuclear species with $A-5$ and $Z-1$ which is transmitted through the FRS as a H-like ion. Although the production cross section for such a contaminant is larger by approximately a factor of 2 than for a nucleus of interest in this region [32], the probability for a H-like charge state is less than 0.5%, resulting in a contamination level of less than 1%.

Further purification of the selected events was achieved by means of signals from the ionization chamber. The atomic number Z of a particle can be estimated by assuming that

$$\Delta E = Z^2 f(\beta). \tag{3}$$

The function f, which depends only on the ion velocity and not on Z, was deduced from the primary beam calibration measurements. The spectrum of Z determined for selected ^{177}Ta events as shown in Figs. 2(a) and 2(b) is plotted in Fig. 2(c). The corresponding spectrum of ^{174}Hf events is also shown for comparison. It can be seen that the resolution of the MUSIC detector is not quite good enough for a completely clean separation of neighboring elements, mainly due to a low-energy tail caused by charge exchange processes in the counter gas. The small shift, resulting in the absolute values of Z appearing not to be calculated exactly, is partially due to a slow drift of the signal amplitude induced by changes in the atmospheric pressure. Nevertheless, by imposing a condition on the MUSIC detector signal, as shown in Fig 2(c), one can strongly suppress any remaining contributions from nuclei with different Z from the specific nuclear species of interest.

The identified ions could still be destroyed due to interactions in the final degrader. The energy-loss signals measured by the SC3 scintillator were used to suppress such events. The resulting spectrum for selected ^{177}Ta ions is shown in Fig. 2(d). Events inside the main peak, which represent about 70% of all counts in the spectrum, are interpreted as those which survived the deceleration process. However, this number should be corrected for neutron knock-out channels (xn-reaction channels), since removal of neutrons does not influence the energy-loss spectrum. The total cross section for the removal of neutrons from the secondary beams in aluminum was estimated by using the abrasion-ablation code ABRABLA [33]. For the case of ^{177}Ta, a value of 450 mb was found. This number yields a correction of about 5% to the final number of stopped ions. Further losses, due to secondary reactions in the SC3 scintillator and in the catcher, were estimated using the total nuclear interaction cross section formula of Benesh, Cook, and Vary [34]. These losses amounted, on average, to approximately 9%. Finally, combining all factors together, we find that only about 60% of ions identified in front of the final degrader survive the slowing down and are stopped in the catcher.

C. Isomer spectroscopy

The ions arriving at the final focus are distributed randomly in time during the spill, and since their total rate was always below 1 kHz, the average time between consecutive ions was larger than 1 ms. The electronic logical gate for gamma detection was only opened for a period of 80 μs after the arrival of a heavy ion, and all subsequent signals from particle and gamma detectors which were read in this time period were stored as a single ''event.'' For each detector, the time between the implantation and an associated detected γ ray (either prompt or delayed) was recorded over two time ranges: 0–8 μs [time-to-digital converter (TDC)] and 0–80 μs [time-to-amplitude converter (TAC)]. This technique allowed the association of isomeric gamma rays with the identified ion, while both room background and radiation from other nuclei are strongly suppressed [5].

The method is sensitive to isomers with half-lives in the range from about 100 ns up to several milliseconds. The lower limit is determined by the time of flight through the FRS (typically approximately 300 ns). However, we note that in some cases this lifetime limit may be considerably lower ($\sim$10 ns) when the electron conversion branch is blocked in a highly stripped ion [5,7,8,23–25,27].

The gamma singles spectrum, summed over all detectors, corresponding to the selection of ^{177}Ta events is shown in Fig. 3 with the condition that the gamma rays were detected between 0.4 and 30 μs after ion implantation in the catcher. Gamma lines depopulating three known isomers in this nucleus [41] are clearly visible, validating the identification methodology.

A quantitative analysis of isomeric ratios requires, in addition to the number of implanted ions, knowledge of the total effective efficiency of the gamma-ray detection array. Since different nuclei were implanted at different locations at the catcher, the dependence of gamma efficiency on the horizontal position must be deduced. Therefore, efficiency curves for each crystal were measured by placing a calibration source at five different positions on both the front and back sides of the catcher, along the central horizontal line. The resulting values from both the front and back were averaged and a parabolic interpolation was applied to determine the efficiency curves $\epsilon_i(x_2)$ for each crystal ($i=1,\ldots,14$) and for any position x_2 of the radiation source.

The stopping of heavy ions in the catcher was accompanied by a prompt burst of radiation, mainly due to x rays and bremsstrahlung. Since the gate for gamma detection allowed

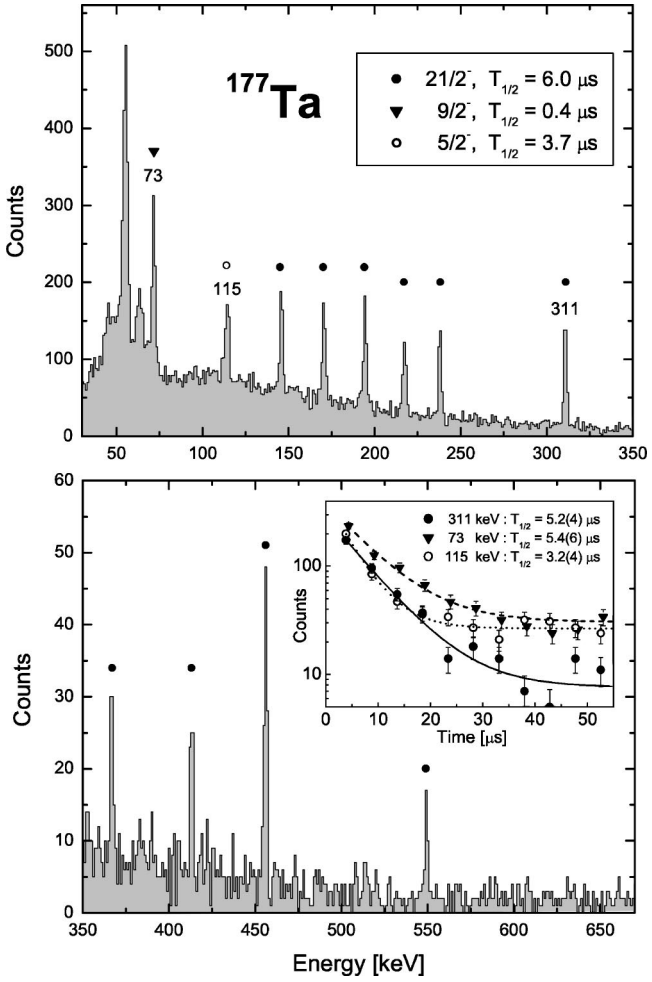

FIG. 3. Singles gamma-ray spectrum corresponding to all ^{177}Ta ions identified as shown in Fig. 2. Spectra from 14 crystals were added with a condition that a gamma ray be detected more than 0.4 μs and less than 30 μs after the arrival of the ion. Gamma transitions from the decay of three previously known isomers in ^{177}Ta are marked. Their spin, parity, and the half-life values [41] are given in the upper panel. The inset in the lower panel shows the measured decay curves for the three gamma lines indicated together with the best fitted curves and the deduced half-lives. Intensities of the 311 keV and 115 keV transitions, depopulating the $21/2^-$ and the $5/2^-$ isomers, respectively, are observed to decay with the half-life consistent with the literature value. Since the $9/2^-$ isomer is fed by the decay of the $21/2^-$ state, the 73 keV transition is observed to decay with the same half-life as the 311 transition.

the recording of prompt radiation and only the first gamma ray in every channel was recorded in an event, the effective efficiency for delayed radiation was reduced. To account for this effect, the probabilities P_i^{burst} for a crystal being ''blinded'' by the burst were determined from the delay-time spectra of each crystal showing the time differences between the ion implantation and the detection of the gamma ray. In each such spectrum a strong peak, representing the prompt events, was seen. It allowed us to set a limit t_{lim} in most cases equal to 0.4 μs, separating the prompt events from the delayed ones. Then, P_i^{burst} is taken as the ratio between the integrated number of counts with delay times shorter than

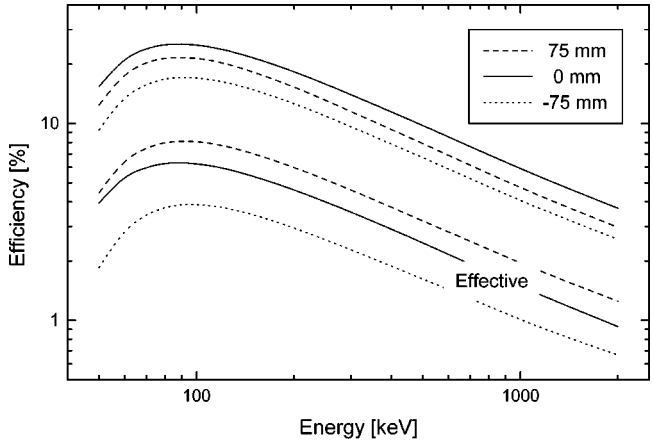

FIG. 4. Efficiency of the gamma-detector array as measured with calibration sources (upper three curves) and corrected for the blocking by a prompt burst (lower curves) at three horizontal positions on the catcher. The effective efficiency curves correspond to ^{174}Hf ($x_2=-75$ mm), ^{177}Ta ($x_2=0$ mm), and ^{181}Re ($x_2=75$ mm).

t_{lim} and the number of identified ions. (Correspondingly, the spectra of delayed gamma rays used to search for isomeric decays were accumulated with the condition that the delay time is larger than t_{lim}.) The total effective efficiency of the gamma array was taken as $\epsilon_{eff}(x_2)=\Sigma_i\epsilon_i(x_2)(1-P_i^{burst})$. The P_i^{burst} values were determined separately for each selected isotope and its average position was used as x_2. Examples of measured ($\Sigma_i\epsilon_i$) and effective (ϵ_{eff}) efficiencies of the full array for three positions of the radiation source are shown in Fig. 4. Clearly, the effect of the prompt burst is large and also alters the position dependence of the effective efficiency. The overall systematic error of the effective efficiency, including the inaccuracy of the averaging and interpolating procedure, as well as the fluctuations of the P_i^{burst} values, was estimated to be 15%.

III. DATA ANALYSIS AND RESULTS

The isomeric ratio R is defined as the probability that in the reaction a nucleus is produced in an isomeric state. We determine it in the following way. First, the observed decay yield is calculated:

$$Y=\frac{N_\gamma(1+\alpha_{tot})}{\epsilon_{eff}b_\gamma}, \tag{4}$$

where N_γ is the number of counts in the gamma line depopulating the isomer of interest, α_{tot} is the total conversion coefficient for this transition, ϵ_{eff} is the effective efficiency, and b_γ is the probability that the decay proceeds through this transition (i.e., the absolute branching ratio). The isomeric ratio is then given by

$$R=\frac{Y}{N_{imp}F\,G}, \tag{5}$$

where N_{imp} is the number of implanted heavy ions, F is a correction factor for the in-flight isomer decay losses, and the factor G corrects for the finite detection time of gamma radiation. The factor F is calculated from

$$F=\exp\left[-\left(\lambda^{q_1}\frac{\mathrm{TOF}_1}{\gamma_1}+\lambda^{q_2}\frac{\mathrm{TOF}_2}{\gamma_2}\right)\right], \tag{6}$$

where TOF_1 (TOF_2) is the time of flight through the first (second) stage of the FRS, γ_1 (γ_2) is the corresponding Lorentz factor, and λ^{q_1} (λ^{q_2}) is the decay constant for the ion in the charge state q_1 (q_2). Since only TOF_2 was measured in the experiment, TOF_1 and γ_1 were calculated using the ion-optical code MOCADI [31]. In this experiment, the transported ions were highly charged (in most of our cases the ions were fully stripped), and the decay constants λ^q can differ considerably from the value for an electrically neutral atom, λ. For the fully stripped ion, λ^0 can be calculated from

$$\lambda^0=\lambda\sum_i\frac{b_{\gamma i}}{1+\alpha_{tot}^i}, \tag{7}$$

where the summation is over all the decay branches depopulating the isomer.

Finally, the correction factor G is calculated using

$$G=\exp(-\lambda\, t_i)-\exp(-\lambda\, t_f), \tag{8}$$

where t_i and t_f are the gamma delay-time limits set in the off-line analysis to produce the delayed gamma spectrum.

When more than one gamma-ray line was observed to depopulate an isomer, the isomeric ratio was calculated separately for the strongest lines and then averaged.

In some cases, more than one isomer in the same nucleus is populated in the reaction and a lower-lying isomer may be partly fed by the delayed decay of a higher-lying metastable state. We adopt here the definition of isomeric ratio as the probability that a state is populated promptly after production of the nucleus in the reaction. Then, it can be shown (see the Appendix) that in a case where the upper state decays with the probability (branching) b_{UL} to the lower one, the isomeric ratio for the latter can be calculated by

$$R_L=\frac{Y_L}{N_{imp}F_LG_L}-b_{UL}\frac{R_U}{F_LG_L}\left[\frac{\lambda_LG_U-\lambda_UG_L}{\lambda_L-\lambda_U}F_U+\frac{\lambda_U^0}{\lambda_L^0-\lambda_U^0}G_L(F_U-F_L)\right], \tag{9}$$

where the indices L and U refer to the lower and upper states, respectively, and the second term on the right side represents the correction due to feeding from the upper state.

In the course of the experiment a number of different FRS settings were applied to study nuclei in three different areas on the Segré chart. The current work concentrates on results from settings centered on (i) the proton drip line in the vicinity of ^{138}Gd, (ii) close to stability around (a) ^{177}Ta and (b) ^{180}Ta, and (iii) around the most neutron-rich tungsten isotope identified to date, ^{191}W. Accurate determination of the isomeric ratios, as follows from the above formulas, requires detailed knowledge of the appropriate decay schemes. Therefore, in the present paper we only report on well-known isomers. Altogether more than 20 such isomers were observed in 18 nuclei. The number of implanted ions ranged from about 2×10^4 in the case of ^{176}Hf to about 7×10^6 in the case of ^{181}Re. The measured gamma spectra of some isomers (^{136}Sm, ^{138}Gd, ^{179}W, ^{200}Pt, and ^{206}Hg) were already published elsewhere (Refs. [13,20–27]). The gamma spectra obtained for all other cases, together with the decay curves for selected gamma lines, fitted using the least squares method, are presented in Figs. 5, 6, and 7.

The properties of isomeric states and the results of the isomeric ratio analysis are given in Table I. The lifetimes of detected isomers were analyzed and in the single-isomer cases were found to be consistent with the published values, but in general with larger error bars. In the current work the published values from references quoted in Table I were used for all cases.

The quoted uncertainties represent the statistical errors added in quadrature to a systematic error of 15%, which arises mainly from the efficiency determination procedure. A cross-check of this procedure was provided by the 6^+ isomer in ^{176}Hf [38] and by the 14^- isomer in ^{180}W [45] which were observed at two different FRS settings: namely, those centered on ^{177}Ta and ^{180}Ta. Although in these two cases the ^{176}Hf and ^{180}W ions were stopped at different positions and, consequently, the effective gamma efficiencies were different, the same values were obtained for the isomeric ratios.

All of the isomers listed in Table I were transmitted through the FRS as fully stripped ions, with the exceptions of ^{200}Pt and ^{206}Hg. These were transmitted as hydrogen- and helium-like ions, respectively, in the second stage of the FRS, when the spectrometer was tuned for fully stripped ^{191}W ions. Also the final degrader was adjusted to achieve the proper implantation of nuclei in the vicinity of ^{191}W. These conditions were not optimal for implantation of much heavier systems like ^{206}Hg. Indeed, the MOCADI simulations showed that ^{206}Hg ions had the shortest range and some of them might have been stopped before reaching the catcher. The very short implantation depth of ^{206}Hg was confirmed by the P_i^{burst} values which were the smallest for this isotope. Hence, our value for the isomeric ratio in this case might be underestimated and should be considered as a lower limit.

The case of ^{200}Pt, which was the most strongly populated isomer in our experiment, is special [23–25,27]. Despite its very short half-life of 14.3 ns [49] it survives the much longer flight time of approximately 300 ns, because, when fully stripped, the effective ionic half-life increases to at least 1 μs due to the blocking of the electron conversion decay branch. The lifetime remains long even when the ion is transmitted in a H-like state, because the energy of the isomeric transition is lower than the K-electron binding energy in platinum (78 keV).

In the four nuclides ^{174}Hf, ^{175}Hf, ^{179}W, and ^{181}W, the decays of two isomers were observed. In the first two cases the decay of the upper state feeds the lower-lying one and

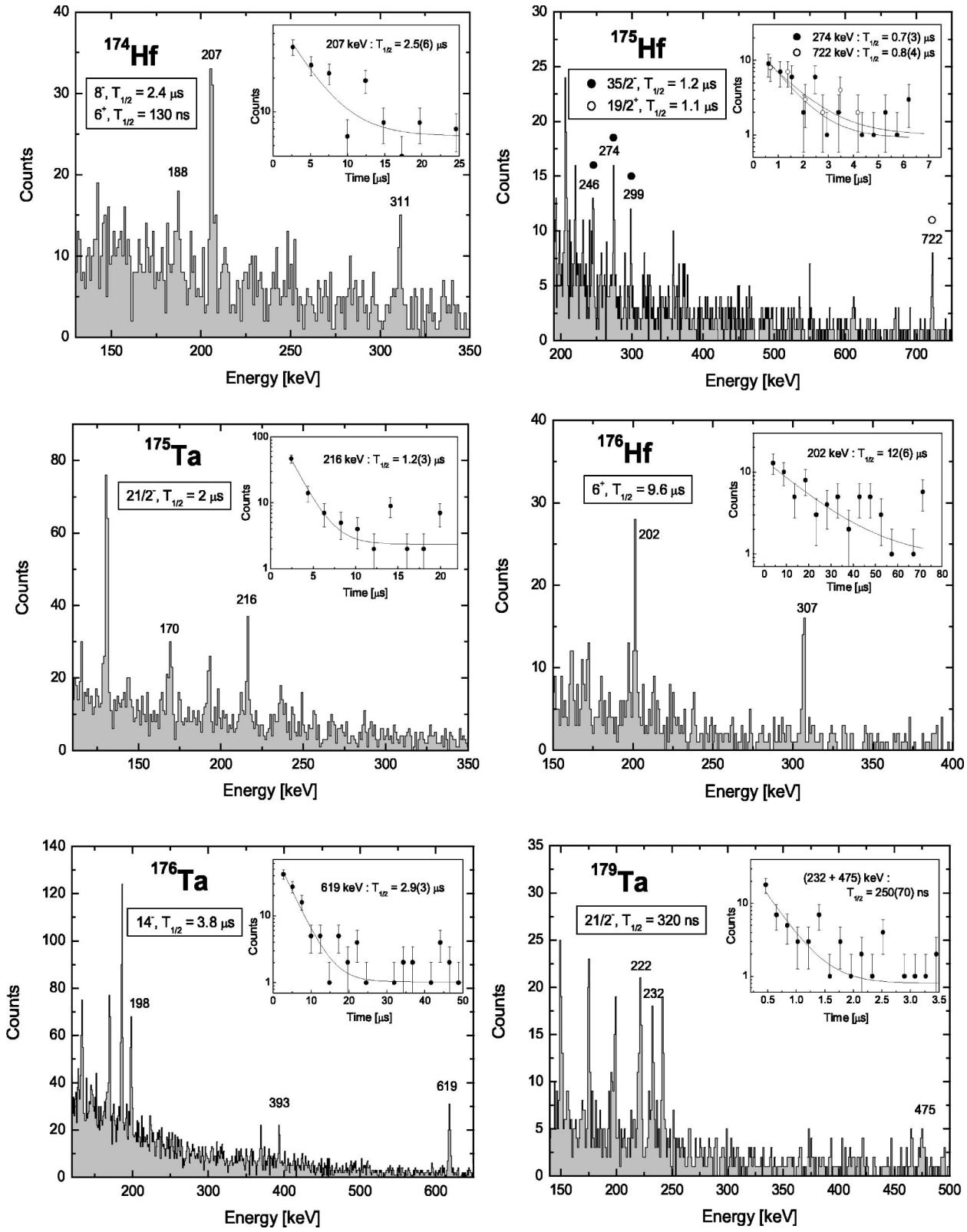

FIG. 5. Singles gamma-ray spectra summed over all crystals, corresponding to the identified heavy ions, as indicated. In each case gamma transitions are seen which originate from the decay of known isomers with the spin, parity, and half-life values given in the box. The transitions marked with their energy in keV were used to determine the isomeric ratios. The insets show the measured decay of the marked transitions together with the fitted decay curves and the deduced half-lives. In the case of ^{174}Hf, the 207 keV line, depopulating the lower-lying, short-lived 6^+ isomer, is observed to decay with the half-life consistent with the value known for the upper 8^- isomer as the result of feeding the 6^+ state in the decay of the 8^- one.

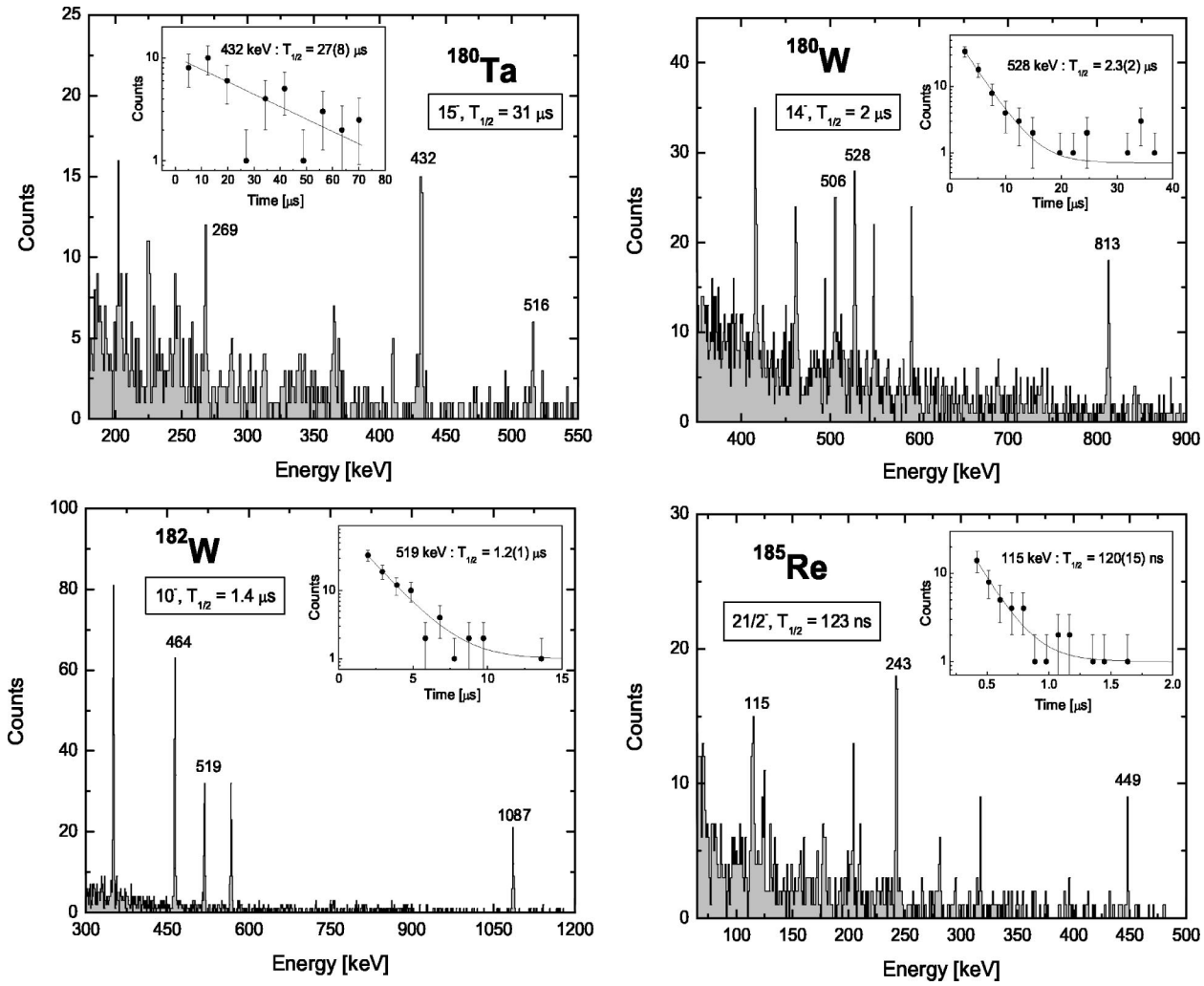

FIG. 6. Singles gamma-ray spectra corresponding to the indicated heavy ions as in Fig. 5.

Eq. (9) had to be used to extract isomeric ratios. For the lower 6^+ state in ^{174}Hf [37], this procedure was rather inaccurate and only an upper limit could be deduced.

In the cases of ^{177}Ta and ^{181}Re the decays of three isomers were detected. For the $9/2^-$ state in ^{177}Ta [41], the correction due to feeding from the $21/2^-$ isomer again yielded an upper limit. The third isomer in this nucleus, which has spin/parity $5/2^-$, is not fed by the decays of the other two and it does not have to be corrected. In ^{181}Re the $25/2^+$ state is fed by the decay of the $35/2^-$ isomer [47], but since the latter is very weakly populated in the reaction, the resulting correction was found to be very small. Thus, the application of the two-level model [Eq. (9)] to the feeding of the $21/2^-$ isomer by the decay of the $25/2^+$ state was justified. Again, only an upper limit can be given.

IV. SHARP CUTOFF MODEL

To describe the population of an isomeric state in a fragmentation reaction we separate the process into two steps. In the ablation phase of the reaction, highly excited prefragments evaporate nucleons until the final fragment is formed with an excitation energy below the particle emission threshold. Subsequently, a statistical gamma cascade proceeds down to the yrast line and then along this line to the ground state. If a long-lived state lies on this decay path, part of the cascade may be hindered or stopped depending on the lifetime of the isomer. The isomeric ratio is equal to the probability that gamma decay from the initial excited fragments proceeds via this isomeric state.

The crucial aspect of the first step is the distribution of the angular momentum in the ensemble of the excited fragments just prior to the gamma deexcitation step. This problem was addressed by de Jong, Ignatyuk, and Schmidt [51] who applied the statistical abrasion-ablation model [33] of fragmentation. Assuming that any angular momentum taken away by evaporating particles is small and can be neglected, they calculated the angular momentum distribution of the final fragment as the superposition of the angular momenta of all prefragments contributing to the final fragment of interest using the ABRABLA code [33]. Furthermore, they have shown that for a large mass difference between the projectile and the fragment this distribution can be approximated by a simple analytical formula

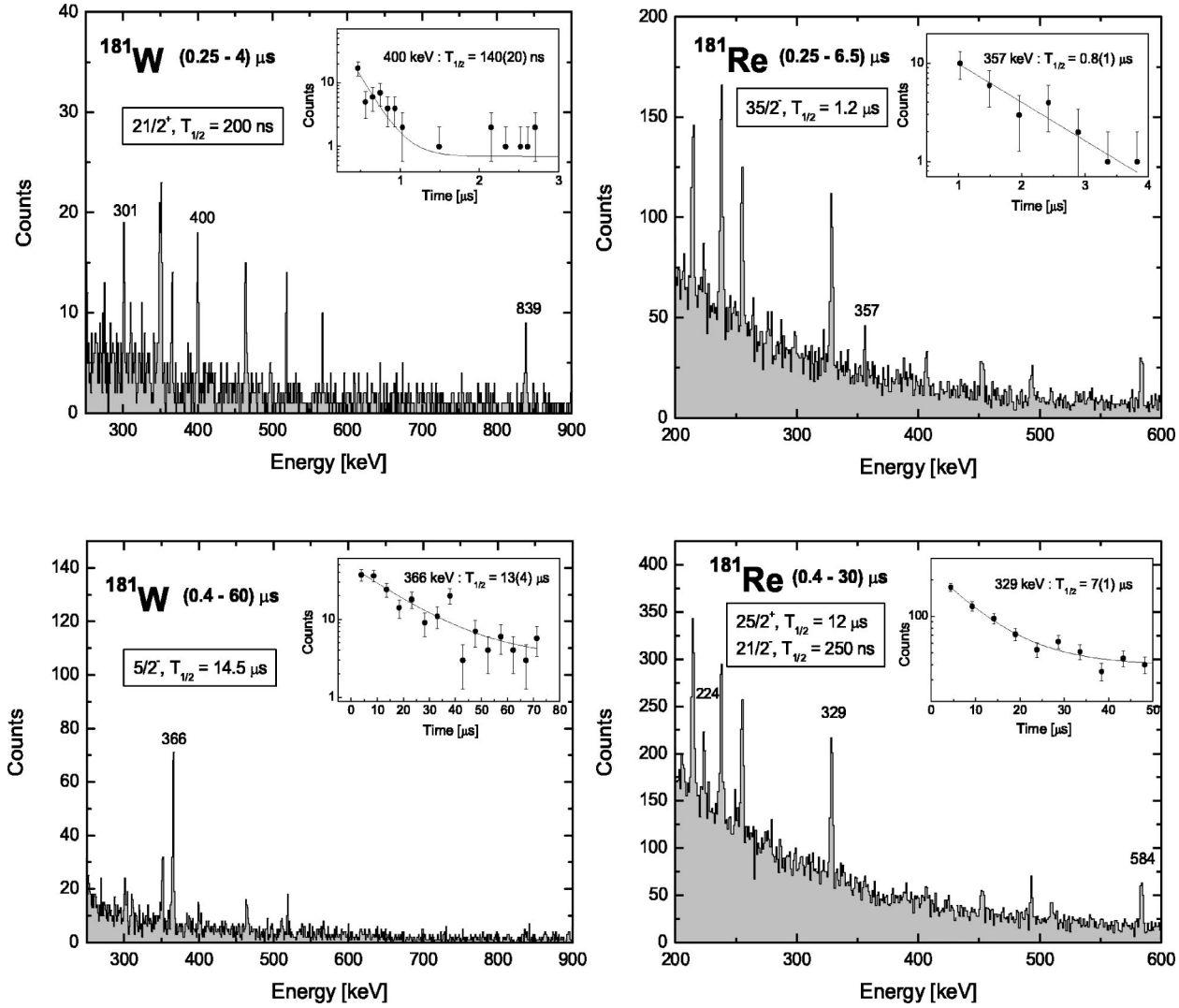

FIG. 7. Gamma transitions from the decay of two different isomers in ^{181}W and ^{181}Re are observed by imposing different conditions on the time interval between the arrival of the ion and the gamma detection, as indicated next to the isotope symbol. The third isomer in ^{181}Re—the short-lived $21/2^-$ state—is fed by the decay of the higher-lying, long-lived $25/2^+$ isomer. As a result, the 329 keV transition, depopulating the $21/2^-$ state, is observed to decay with a long half-life consistent with that of the $25/2^+$ isomer.

$$P_J = \frac{2J+1}{2\sigma_f^2}\exp\left[-\frac{J(J+1)}{2\sigma_f^2}\right], \tag{10}$$

where σ_f, the so-called spin-cutoff parameter of the final fragments, is given by

$$\sigma_f^2 = \langle j_z^2\rangle \frac{(A_p - A_f)(\nu A_p + A_f)}{(\nu+1)^2(A_p-1)}. \tag{11}$$

A_p and A_f denote the projectile and fragment mass numbers, respectively, ν is the mean number of evaporated nucleons per abraded mass unit, and $\langle j_z^2\rangle$ is the average square of the angular momentum projection of a nucleon in the nucleus. It is generally assumed that the abrasion of one nucleon induces an excitation energy of about 27 MeV [52], whereas the evaporation of a nucleon decreases the energy by about 13 MeV; hence, the parameter $\nu = 2$ is taken. Values of $\langle j_z^2\rangle$ can be estimated on the basis of a semiclassical consideration of the angular momentum distribution in the Woods-Saxon potential [53,51] following

$$\langle j_z^2\rangle = 0.16\, A_p^{2/3}\left(1 - \frac{2}{3}\beta\right), \tag{12}$$

where β is the quadrupole deformation parameter. Angular momentum distributions calculated with the ABRABLA code for three selected fragments are shown in Fig. 8 together with the results of the approximation given by Eqs. (10)–(12). It is seen that for ^{206}Hg and ^{200}Pt (the two fragments closest to the ^{208}Pb projectile in our data set) the approximate formula fails to agree with the results of the full numerical calculations. On the other hand, in the case of ^{185}Re the approximation reproduces the ABRABLA result with good accuracy. Since the same (or better) agreement was found for all other cases considered, which differ from the projectile in

TABLE I. List of isomers analysed in the present work. For each nucleus the spin, parity, excitation energy, energy difference from the yrast line, adopted deformation parameter (β), and the half-life of the corresponding isomer are given, followed by the experimentally determined isomeric ratio (see text) and a value predicted by the sharp cutoff model. The decay scheme data were taken from the references indicated next to the isotope symbol.

Nucleus	I^π	E^* [keV]	ΔE [keV]	β	$T_{1/2}$ [μs]	R_{expt} [%]	R_{th} [%]
^{136}Sm [35]	8^-	2265	466	0.23	15	3.5(1.2)	70.2
^{138}Gd [36]	8^-	2233	583	0.24	6	5.0(1.0)	69.3
^{174}Hf [37]	8^-	1798	788	0.24	2.4	2.0(5)	49.3
	6^+	1549	941	0.24	0.133	<6	66.2
^{175}Hf [37]	$35/2^-$	3016	0	0.24	1.21	2.5(6)	3.8
	$19/2^+$	1434	537	0.24	1.10	3(1)	36.5
^{176}Hf [38]	6^+	1333	736	0.24	9.5	6(2)	64.4
^{175}Ta [39]	$21/2^-$	1566	624	0.24	2.0	2.0(5)	29.5
^{176}Ta [40]	14^-	1372	147	0.25	3.8	2.6(5)	11.0
^{177}Ta [41]	$21/2^-$	1355	344	0.25	6.0	9(2)	27.1
	$9/2^-$	73	0	0.25	0.41	<4	76.5
	$5/2^-$ [a]	186	115	0.25	3.7	4.0(6)	91.0
^{179}Ta [42]	$21/2^-$	1252	0	0.25	0.32	9(3)	24.9
^{180}Ta [43]	15^-	520	0	0.22	31	10(3)	6.1
^{179}W [44]	$35/2^-$	3348	21	0.25	0.75	2.7(5)	2.4
	$21/2^+$	1632	509	0.25	0.39	6(1)	25.7
^{180}W [45]	14^-	3263	440	0.21	2	6.4(10)	8.9
^{181}W [45]	$21/2^+$	1653	614	0.21	0.2	17(4)	23.6
	$5/2^-$ [a]	366	0	0.21	14.5	6(1)	90.1
^{182}W [46]	10^+	2230	518	0.21	1.4	10(2)	25.6
^{181}Re [47]	$35/2^-$	3869	521	0.22	1.2	0.2(1)	2.0
	$25/2^+$	1881	191	0.22	12	2.8(5)	13.1
	$21/2^-$	1656	447	0.22	0.250	<3	23.4
^{185}Re [48]	$(21/2^-)$	2124	261	0.21	0.123	21(6)	18.6
^{200}Pt [49]	7^-	1617	0	0	0.014	30(5)	35.5
^{206}Hg [50]	5^-	2102	0	0	2.15	3.7(7)	32.5

[a]The spin of the isomer is lower than the spin of the ground state.

mass by more than ^{185}Re, in the following we use the analytical approximation for all nuclei, except for the two heaviest ones (^{206}Hg and ^{200}Pt).

Given the angular momentum distribution of the final fragment, one can consider the probability that gamma decays will lead to an isomeric state of spin J_m. First, we assume that the initial excitation energies are well above the excitation energy of the isomer. All the observed isomers described in the current work lie below 4 MeV in excitation energy (see Table I), while the particle emission threshold for these nuclei is of the order of 8 MeV. Second, we make the extreme simplifying assumption that *all* states with $J \geqslant J_m$, and only those, decay to the isomer. A similar approach, known in the literature as the ''sharp cutoff model,'' has been used in studies of angular momentum distributions in compound nuclei [54–56] and in fission fragments [57]. From Eq. (10) it follows that

$$R_{th} = \int_{J_m}^{\infty} P_J dJ = \exp\left[-\frac{J_m(J_m+1)}{2\sigma_f^2} \right]. \qquad (13)$$

Substituting $\nu = 2$ and introducing $\Delta A = A_p - A_f$, Eqs. (11) and (12) yield

$$\sigma_f^2 = 0.0178\left(1 - \frac{2}{3}\beta\right) A_p^{2/3} \frac{\Delta A(3A_p - \Delta A)}{A_p - 1}. \qquad (14)$$

One might expect that the assumptions leading to Eq. (13) may be justified only for isomers lying close to the yrast line and that the isomeric ratio should decrease with increasing energy difference between the isomer and the yrast line.

Isomeric ratios, calculated as described above, for the cases observed are given in Table I. The deformation parameters were taken from Ref. [58] where available or were estimated from the systematics [59].

V. DISCUSSION

The inspection of the last two columns of Table I reveals that only in seven cases is the agreement between the sharp cutoff model and experiment satisfactory. In all other cases the model overestimates the isomeric ratios.

First, we note the exceptional character of $5/2^-$ isomers in

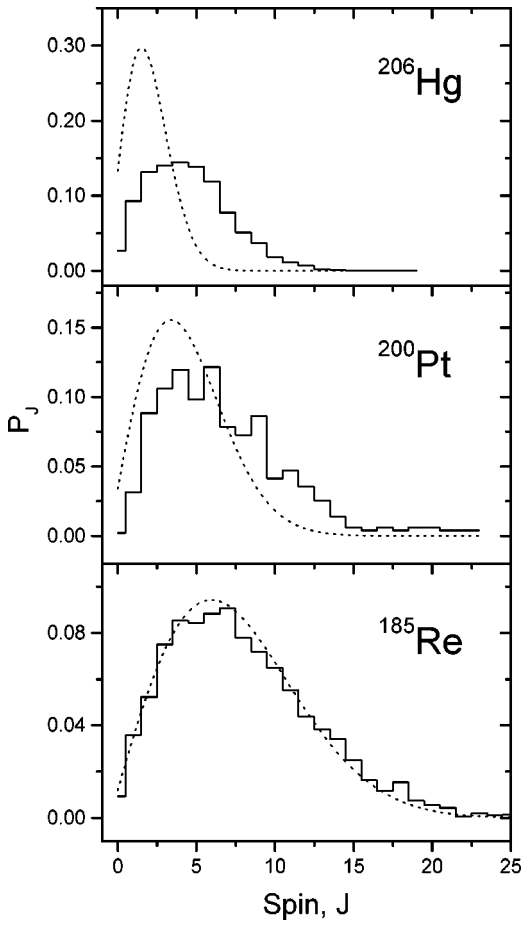

FIG. 8. Angular momentum distributions in the final products of the fragmentation of 1 GeV/nucleon ^{208}Pb beam on a beryllium target calculated with the ABRABLA code [33] (solid line histogram) compared with the predictions of the analytical approximation described in the text (dashed curve). All distributions are normalized to the integral value of 1.

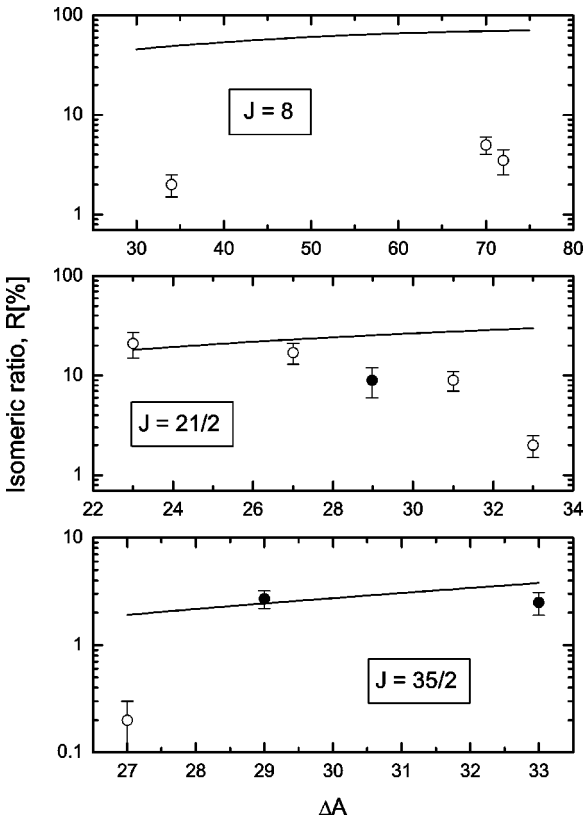

FIG. 9. Measured isomeric ratios as a function of mass difference ΔA between the projectile and the fragment for three values of isomeric spin compared with predictions of the sharp cutoff model. The solid points indicate isomers located on the yrast line or very close to it. The deformation parameter β was assumed to be 0.23, 0.23, and 0.24 for $J=8$, 21/2, and 35/2, respectively.

^{177}Ta and in ^{181}W. In these cases, the spin of the isomer is lower than the spin of the ground state. These isomers are very weakly populated presumably because they are not situated on the main flow of the gamma cascade which proceeds along the yrast line and stops, most likely, at the ground state. Such a scenario is not within the scope of the sharp cutoff model, whose prediction of large isomeric ratios in these cases ($\simeq$90%) simply reflects the low value of the spin.

Next, it should be pointed out that in those cases where more than one isomer was observed, the isomeric ratios obtained experimentally for the lower-lying states generally cannot be compared with the model because its assumption that all states with the higher spin decay promptly to the isomer of interest is explicitly violated. In principle, in those cases where the higher-lying isomer decays to the lower state, like in ^{174}Hf, ^{175}Hf, ^{177}Ta, and ^{181}Re, one could add the two (or three) measured isomeric ratios to compare with the prediction for the lowest state. Although this procedure reduces the observed discrepancies between the model and the experiment in these cases, it does not help to understand them because already the higher-lying state is not properly described by the model. Moreover, in the cases where two isomers are not connected by the decay path, like in ^{179}W, such procedure is not justified. Therefore, we concentrate in the following discussion only on the highest-lying identified states.

We also exclude the case of ^{206}Hg. The model based on the full ABRABLA calculation overestimates the isomeric ratio for the 5^- (yrast) state in this nucleus [50] by almost an order of magnitude. This could be the effect of the incorrect implantation of this nucleus resulting in the underestimated value of the measured isomeric ratio, as discussed in Sec. III.

The prediction of the sharp cutoff model depends on the spin of the isomer, on the mass difference between the projectile and the final fragment, and on the deformation parameter β. Plots of selected isomeric ratios versus mass difference (ΔA), for the constant value of spin J, are shown in Fig. 9 for the three cases of $J=8$, $J=21/2$, and $J=35/2$ together with model predictions. In each group of given J all points are associated with a similar value of deformation parameter β and hence a constant β value was adopted in calculating the predictions for each spin.

It turns out that in each case the experimental points are located close to or below the theoretical lines. We observe that the three data points for $J=8$, which differ from the

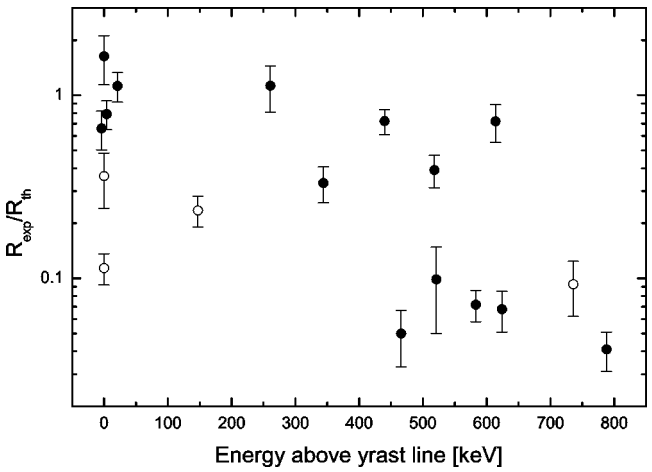

FIG. 10. Ratios of the measured isomeric ratio to the value predicted by the sharp cutoff model plotted vs the energy difference between the isomer and the yrast line. In nuclei where two isomers were measured, only the higher-lying state is included. Open points indicate cases where higher-lying, long-lived isomers are known, but could not be identified in the present measurement because of too short observation time (TAC range).

predicted value by a factor of about 20, represent isomers lying more than 450 keV above the yrast line. In the case of the $J=35/2$ isomer in ^{181}Re [47] (which is nonyrast by 521 keV), the experimental isomeric ratio is, again, smaller than the model prediction by a factor of 10 while the two other results which are yrast or very close to yrast (^{179}W [44] and ^{175}Hf [37]) agree well with the model. Note that these three isomers represent the highest discrete spin observed to date in fragmentation reactions. In contrast, this tendency is not supported by $J=21/2$ isomers. For the only yrast case—namely, ^{179}Ta [42]—the measured isomeric ratio is nearly 3 times smaller than the prediction, while the two points which are in a good agreement with the model, corresponding to ^{185}Re [48] and ^{181}W [45], are nonyrast by 261 keV and 614 keV, respectively. The reduction of the isomeric ratio in the case of ^{179}Ta could be explained by the existence of a long-lived isomer ($T_{1/2}=11$ ms, $J^{\pi}=25/2^{+}$) located just above (65 keV) the $21/2^{-}$ state [42]. If a substantial part of the gamma cascade is trapped in this long-lived state, the feeding of the observed 21/2 isomer will be negligible in the relatively short observation time. In this nucleus, however, there is another isomer which should be populated and observed as well ($23/2^{-}$, $T_{1/2}=1.6$ μs, yrast), located about 75 keV above the $21/2^{-}$ state and decaying to it [42]. Surprisingly, we see neither the 75 keV transition depopulating the $23/2^{-}$ isomer nor its influence on the decay pattern of the 232 keV and 475 keV lines depopulating the $21/2^{-}$ state (see Fig. 5).

In the following, we will concentrate our discussion on how isomeric ratios are influenced by the energy difference between the isomeric state and the yrast line. In individual cases, however, nuclear structure effects such as the trapping of the gamma cascade by specific higher-lying isomeric states which are too long-lived to be detected in the present experiment or details of the decay branching pattern close to the yrast line, may of course also strongly affect the isomeric ratio.

Figure 10 shows the ratio R_{expt}/R_{th} versus the excitation energy of the isomer above the yrast state of the same spin in that particular nucleus. Open symbols indicate those cases where a higher-lying, long-lived isomer (not observed in our experiment) is known to exist, which may reduce the feeding of the isomers we observe by delaying part of the gamma cascade. With the exception of ^{179}Ta, which was discussed above, these cases include ^{176}Ta, where an $I^{\pi}=20^{-}$, $T_{1/2}=1$ ms isomer has been reported [40] above the 14^{-} state observed in the current work, and ^{176}Hf, where both $I^{\pi}=14^{-}$, $T_{1/2}=400$ μs and $I^{\pi}=8^{-}$, $T_{1/2}=9.8$ μs isomers are located [38] above the measured 6^{+} state. Indeed, isomeric ratios in these cases appear to be reduced with respect to the model. Despite these complications, it is evident that the overall trend is one of decreasing isomeric ratio with increasing energy above the yrast line.

The data points in Fig. 10 are grouped in two rather separate regions. In the first group, which represents results close to the model prediction, a decrease of the R_{expt}/R_{th} ratio with increasing energy from the yrast line is observed. The isomeric ratio is reduced by a factor of about 2 at 700 keV above the yrast line. The second group represents isomers far from the yrast line, which correspond to the smallest observed values of R_{expt} (less than 10% of the model prediction). The strong reduction in the isomeric ratio for ^{174}Hf which belongs to this group (open point) may be explained by two independent factors: (a) the fact that it lies a long way from the yrast line and (b) the presence of the higher-lying, long-lived isomer. One might suspect that for other nuclei in this group, long-lived isomeric states, as yet unobserved, are present.

Finally, the sharp cutoff model is observed to represent the upper limit for the isomeric ratio. Its key assumption concerning the flow of the gamma cascade following the formation of the fragment is very crude and is particularly limiting in case of nuclei with such a rich structure of isomers like the region of K isomers investigated in this work. Generally, the predictions of the model are more accurate for the yrast states—out of seven cases in which good agreement between the model and the experiment is found, five are yrast states. However, exceptions from this rule are observed. The 14^{-} state in ^{180}W and $21/2^{+}$ in ^{181}W are both far from the yrast line, yet their population probability agrees well with the prediction. On the other hand, the $9/2^{-}$ isomer in ^{177}Ta, although yrast, is apparently omitted by the main flow of the gamma cascade and its population is found to be much weaker that for the higher-lying, nonyrast $21/2^{-}$ state. Evidently other nuclear structure effects influencing the detailed branching scheme are responsible for such strong deviations from the model in the individual cases.

VI. SUMMARY

In summary, we have measured the isomeric ratios for more than 20 isomers, ranging in mass between $A=136$ and 206, produced in the fragmentation of a ^{208}Pb beam at 1 GeV/nucleon. These isomers show a wide distribution in an-

gular momenta, ranging from $\frac{5}{2}\hbar$ up to $\frac{35}{2}\hbar$. The latter represents the largest discrete spin observed to date in fragmentation reactions. A simple model of the isomer population is described. It is based on the initial angular momentum distribution in a projectile fragment, as given by the statistical abrasion-ablation model of the fragmentation, and on the assumption that all initial states with higher spin values than the isomer subsequently decay to it. The predictions of this model are found to give an upper limit for the measured isomeric ratios. It is observed that the population probability for an isomer is generally reduced if it is located far from the yrast line.

ACKNOWLEDGMENTS

The excellent work of the SIS synchrotron staff providing a high-intensity primary beam is acknowledged. This work was supported by the Engineering and Physical Sciences Research Council (U.K.), Polish Committee of Scientific Research under Grant No. KBN 2 P03B 036 15, U.S. Department of Energy Contract No. DE-FG02-96ER40983, the EU Access to Large Scale Facilities Program, and the Swedish Natural Sciences Research Council. The clover detectors are funded by CEA (France), EPSRC (U.K.), GSI (Germany), and NBI (Denmark). We are grateful to Dr. Geirr Sletten for use of the NBI EXOGAM clover detector for this experiment.

APPENDIX

We consider a nucleus having two isomeric states referred to as the upper (U) and the lower (L). The upper state decays to the lower one with a probability (absolute branching) b_{UL}. Assume that out of N_0 such nuclei produced at time $t=0$, $R_U N_0$ are found in the upper state and $R_L N_0$ in the lower one, where R_U and R_L denote the corresponding isomeric ratios. The time dependence of the number of upper and lower isomers [$N_U^m(t)$ and $N_L^m(t)$] is given by the following differential equations:

$$\frac{dN_U^m(t)}{dt} = -\lambda_U^q N_U^m(t), \tag{A1}$$

$$\frac{dN_L^m(t)}{dt} = -\lambda_L^q N_L^m(t) + b_{UL}\lambda_U^q N_U^m(t), \tag{A2}$$

with the initial conditions $N_U^m(0)=R_U N_0$ and $N_L^m(0)=R_L N_0$. The decay constant λ^q depends on the charge state of an ion and thus it is different for an ion in flight (stripped) and for an ion at rest (neutral). For the sake of simplicity we assume in the following that $\lambda^q=\lambda^0$ for $0<t\leqslant$TOF and $\lambda^q=\lambda$ for $t>$TOF; i.e., an ion is fully stripped during the TOF and neutral after stopping.

The solution of Eq. (A1) reads

$$N_U^m(t) = \begin{cases} R_1 N_0 e^{-\lambda_U^0 t} & \text{for } 0<t\leqslant \text{TOF}, \\ R_1 N_0 e^{-\lambda_U^0 TOF} e^{-\lambda_U (t-TOF)} & \text{for } t\geqslant \text{TOF}. \end{cases} \tag{A3}$$

The number of decays of the upper isomer (the yield) within the observation time limits $\text{TOF}+t_i<t<\text{TOF}+t_f$, at the end of the separator, is given by

$$Y_U = T\int_{TOF+t_i}^{TOF+t_f} \lambda_U N_U^m(t)dt = R_U N_{imp} F_U G_U, \tag{A4}$$

where T is the total transmission of ions through the separator, $N_{imp}=TN_0$ is the number of ions implanted in the stopper and correction factors $F_U=e^{-\lambda_U^0 TOF}$ and $G_U=e^{-\lambda_U t_i}-e^{-\lambda_U t_f}$ were introduced for the in-flight decay losses and for the finite detection time, respectively. The necessary modification of the factor F due to relativistic time dilation and varying velocity in the spectrometer are straightforward [see Eq. (6)].

Now, Eq. (A2) is solved after substituting for $N_U^m(t)$ the solutions (A3) and (A4). For $0<t\leqslant$TOF one gets

$$N_L^m(t) = R_L N_0 e^{-\lambda_L^0 t} + R_U N_0 b_{UL}\frac{\lambda_U^0}{\lambda_L^0-\lambda_U^0}(e^{-\lambda_U^0 t}-e^{-\lambda_L^0 t}), \tag{A5}$$

which for $t=$TOF reduces to

$$N_L^m(\text{TOF}) = R_L N_0 F_L + R_U N_0 b_{UL}\frac{\lambda_U^0}{\lambda_L^0-\lambda_U^0}(F_U-F_L). \tag{A6}$$

The solution for $t\geqslant$TOF reads

$$\begin{aligned} N_L^m(t) = {} & R_L N_0 F_L e^{-\lambda_L (t-TOF)} + R_U N_0 b_{UL}\left\{\frac{\lambda_U^0}{\lambda_L^0-\lambda_U^0}\right. \\ & \times (F_U-F_L)e^{-\lambda_L (t-TOF)} - \frac{\lambda_U}{\lambda_L-\lambda_U} \\ & \left.\times F_U[e^{-\lambda_L (t-TOF)} - e^{-\lambda_U (t-TOF)}]\right\}. \end{aligned} \tag{A7}$$

The yield of the lower isomer is then calculated:

$$\begin{aligned} Y_L = {} & T\int_{TOF+t_i}^{TOF+t_f}\lambda_L N_L^m(t)dt = R_L N_{imp} F_L G_L \\ & + R_U N_{imp} b_{UL}\left[\frac{\lambda_L G_U - \lambda_U G_L}{\lambda_L-\lambda_U}F_U\right. \\ & \left. + \frac{\lambda_U^0}{\lambda_L^0-\lambda_U^0}G_L(F_U-F_L)\right], \end{aligned} \tag{A8}$$

from which Eq. (9) follows directly.

[1] R. Schneider *et al.*, Z. Phys. A **348**, 241 (1994); M. Lewitowicz *et al.*, Phys. Lett. B **332**, 20 (1994).
[2] Ch. Engelmann *et al.*, Z. Phys. A **352**, 351 (1995).
[3] B. Blank *et al.*, Phys. Rev. Lett. **84**, 1116 (2000).
[4] B.M. Young *et al.*, Phys. Lett. B **311**, 22 (1993).
[5] R. Grzywacz *et al.*, Phys. Lett. B **355**, 439 (1995).
[6] R. Grzywacz *et al.*, Phys. Rev. C **55**, 1126 (1997).
[7] C. Chandler *et al.*, Phys. Rev. C **56**, R2924 (1997).
[8] C. Chandler *et al.*, Phys. Rev. C **61**, 044309 (2000).
[9] M. Lewitowicz *et al.*, Nucl. Phys. **A682**, 175 (2001).
[10] W.-D. Schmidt-Ott *et al.*, Z. Phys. A **350**, 215 (1994).
[11] M. Pfützner *et al.*, Phys. Lett. B **444**, 32 (1998).
[12] J.M. Daugas *et al.*, Phys. Lett. B **476**, 213 (2000).
[13] Zs. Podolyák *et al.*, Phys. Lett. B **491**, 225 (2000).
[14] T. Enqvist *et al.*, Nucl. Phys. **A658**, 47 (1999).
[15] J. Benlliure, K.-H. Schmidt, D. Cortina-Gil, T. Enqvist, F. Farget, A. Heinz, A.R. Junghans, J. Pereira, and J. Taieb, Nucl. Phys. **A660**, 87 (1999).
[16] K. Sümmerer and B. Blank, Phys. Rev. C **61**, 034607 (2000), and references therein.
[17] J.M. Daugas, Ph.D. thesis, Université de Caen, 1999.
[18] J.M. Daugas, R. Grzywacz, M. Lewitowicz, M.J. Lopez-Jimenes, F. de Oliveira-Santos, J.C. Angélique, L. Axelsson, C. Borcea, C. Longour, and G. Neyens, Phys. Rev. C **63**, 064609 (2001).
[19] M. Pfützner, R. Grzywacz, M. Lewitowicz, and K. Rykaczewski, Nucl. Phys. **A626**, 259c (1997), and references therein.
[20] Ch. Schlegel *et al.*, Phys. Scr. **T88**, 72 (2000).
[21] M. Pfützner, P.H. Regan, Zs. Podolyák, J. Gerl, M. Hellström, M. Caamaño, P. Mayet, M. Mineva, M. Sawicka, and Ch. Schlegel, in *Experimental Nuclear Physics in Europe*, edited by B. Rubio, M. Lozano, and W. Gelletly, AIP Conf. Proc. No. 495 (AIP, Melville, NY, 1999), p. 113.
[22] Zs. Podolyák, P.H. Regan, M. Pfützner, J. Gerl, M. Hellström, M. Caamaño, P. Mayet, M. Mineva, M. Sawicka, and Ch. Schlegel, in *Proceedings of the Second International Conference on Fission and Properties of Neutron-Rich Nuclei*, St. Andrews, Scotland, 1999, edited by J.H. Hamilton, W.R. Phillips, and H.K. Carter (World Scientific, London, 1999), p. 156.
[23] M. Caamaño *et al.*, Acta Phys. Pol. B **32**, 763 (2001).
[24] M. Caamaño, P.H. Regan, Zs. Podolyák, C.J. Pearson, P. Mayet, J. Gerl, Ch. Schlegel, M. Pfützner, M. Hellström, and M. Mineva, Nucl. Phys. **A682**, 223 (2001).
[25] Zs. Podolyák, P.H. Regan, M. Caamaño, J. Gerl, P. Mayet, Ch. Schlegel, M. Hellström, M. Mineva, and M. Pfützner, in *Proceedings of the International Conference "Structure of the Nucleus at the Dawn of the New Century": Nuclear Structure*, Bologna, Italy, 2000, edited by G.C. Bonsignori, M. Bruno, A. Ventura, and D. Vretenar (World Scientific, London, 2000), p. 298.
[26] Zs. Podolyák, P.H. Regan, P.M. Walker, M. Caamaño, P. Mayet, J. Gerl, Ch. Schlegel, M. Hellström, M. Mineva, and M. Pfützner, Proceedings of the International Conference "Exotic Nuclei at the Proton-Drip Line," Camerino, Italy, 2001 (in press).
[27] Zs. Podolyák, M. Caamaño, P.H. Regan, P.M. Walker, P. Mayet, J. Gerl, Ch. Schlegel, M. Hellström, M. Mineva, and M. Pfützner, Prog. Theor. Phys. (to be published).
[28] H. Geissel *et al.*, Nucl. Instrum. Methods Phys. Res. B **70**, 286 (1992).
[29] C. Scheidenberger, Th. Stöhlker, W.E. Meyerhof, H. Geissel, P.H. Mokler, and B. Blank, Nucl. Instrum. Methods Phys. Res. B **142**, 441 (1998).
[30] J. Simpson *et al.*, Heavy Ion Phys. **11**, 159 (2000).
[31] N. Iwasa *et al.*, Nucl. Instrum. Methods Phys. Res. B **126**, 284 (1997).
[32] M. de Jong *et al.*, Nucl. Phys. **A628**, 479 (1998).
[33] J.-J. Gaimard and K.-H. Schmidt, Nucl. Phys. **A531**, 709 (1991).
[34] C.J. Benesh, B.C. Cook, and J.P. Vary, Phys. Rev. C **40**, 1198 (1989).
[35] A.M. Bruce, P.M. Walker, P.H. Regan, G.D. Dracoulis, A.P. Byrne, T. Kibédi, G.J. Lane, and K.C. Yeung, Phys. Rev. C **50**, 480 (1994).
[36] A.M. Bruce, A.P. Byrne, G.D. Dracoulis, W. Gelletly, T. Kibédi, F.G. Kondev, C.S. Purry, P.H. Regan, C. Thwaites, and P.M. Walker, Phys. Rev. C **55**, 620 (1997).
[37] N.L. Gjørup, P.M. Walker, G. Sletten, M.A. Bentley, B. Fabricius, and J.F. Sharpey-Schafer, Nucl. Phys. **A582**, 369 (1995).
[38] T.L. Khoo, F.M. Bernthal, R.A. Warner, G.E. Bertsch, and G. Hamilton, Phys. Rev. Lett. **35**, 1256 (1975).
[39] F.G. Kondev *et al.*, Nucl. Phys. **A601**, 195 (1996).
[40] F.G. Kondev, G.D. Dracoulis, A.P. Byrne, and T. Kibédi, Nucl. Phys. **A632**, 473 (1998).
[41] M. Dasgupta, G.D. Dracoulis, P.M. Walker, A.P. Byrne, T. Kibédi, F.G. Kondev, G.J. Lane, and P.H. Regan, Phys. Rev. C **61**, 044321 (2000).
[42] F.G. Kondev, G.D. Dracoulis, A.P. Byrne, T. Kibédi, and S. Bayer, Nucl. Phys. **A617**, 91 (1997).
[43] G.D. Dracoulis, S.M. Mullins, A.P. Byrne, F.G. Kondev, T. Kibédi, S. Bayer, G.J. Lane, T.R. McGoram, and P.M. Davidson, Phys. Rev. C **58**, 1444 (1998); G.D. Dracoulis, F.G. Kondev, A.P. Byrne, T. Kibédi, S. Bayer, P.M. Davidson, P.M. Walker, C. Purry, and C.J. Pearson, *ibid.* **53**, 1205 (1996).
[44] P.M. Walker, G.D. Dracoulis, A.P. Byrne, B. Fabricius, T. Kibédi, A.E. Stuchbery, and N. Rowley, Nucl. Phys. **A568**, 397 (1994).
[45] D. Yeung, Ph.D. thesis, Univerity of Surrey, 1994.
[46] T. Shizuma, S. Mitarai, G. Sletten, R.A. Bark, N.L. Gjørup, H.J. Jensen, J. Wrzesinski, and M. Piiparinen, Nucl. Phys. **A593**, 247 (1995).
[47] C.J. Pearson, P.M. Walker, C.S. Purry, G.D. Dracoulis, S. Bayer, A.P. Byrne, T. Kibédi, and F.G. Kondev, Nucl. Phys. **A674**, 301 (2000).
[48] T. Shizuma, G. Sletten, R.A. Bark, N.L. Gjørup, H.J. Jensen, S. Mitarai, M. Piiparinen, and J. Wrzesinski, Z. Phys. A **359**, 229 (1997).
[49] S.Y. Yates, E.M. Baum, E.A. Henry, L.G. Mann, N. Roy, A. Aprahamian, R.A. Meyer, and R. Estép, Phys. Rev. C **37**, 1889 (1988).
[50] G.J. Lane *et al.*, Nucl. Phys. **A682**, 71 (2001).
[51] M. de Jong, A.V. Ignatyuk, and K.-H. Schmidt, Nucl. Phys. **A613**, 435 (1997).
[52] K.-H. Schmidt *et al.*, Phys. Lett. B **300**, 313 (1993).
[53] A.V. Ignatyuk, *Statistical Properties of Excited Nuclei* (Energoatomizdat, Moscow, 1983).

[54] J.R. Huizenga and R. Vandenbosch, Phys. Rev. **120**, 1305 (1960).
[55] R. Vandenbosh and J.R. Huizenga, Phys. Rev. **120**, 1313 (1960).
[56] I.S. Grant and M. Rathle, J. Phys. G **5**, 1741 (1979), and references therein.
[57] H. Naik, S.P. Dange, R.J. Singh, S.K. Das, and R. Guin, Nucl. Phys. **A648**, 45 (1999), and references therein.
[58] W. Nazarewicz, M.A. Riley, and J.D. Garrett, Nucl. Phys. **A512**, 61 (1990).
[59] S. Raman, C.W. Nestor, S. Kahane, K.H. Bhatt, and At. Data, At. Data Nucl. Data Tables **42**, 1 (1989).